Influence of TiO$_2$ dispersion on silica support toward enhanced amine assisted CO$_2$ photoconversion to methanol

N.F. Khusnun [a], A.A. Jalil [a,b,*], T.A.T. Abdullah [a,b], S.S.M. Latip [a], C.N.C. Hitam [a], A.A. Fauzi [a], N. S. Hassan [a], M.A.H. Aziz [c], A.F.A. Rahman [a], F.F.A. Aziz [a], M. Bahari [c], R.H. Adnan [c], R. Saravanan [d]

[a] School of Chemical and Energy Engineering, Universiti Teknologi Malaysia, 81310 UTM Johor Bahru, Johor, Malaysia
[b] Centre of Hydrogen Energy, Institute of Future Energy, Universiti Teknologi Malaysia, 81310 UTM Johor Bahru, Johor, Malaysia
[c] Faculty of Science, Universiti Teknologi Malaysia, 81310 UTM Johor Bahru, Johor, Malaysia
[d] Department of Mechanical Engineering, University of Tarapacá, Avda. General Velasquez, 1775 Arica, Chile

ABSTRACT

In this work, titania-supported fibrous silica (TiO$_2$-KCC1) and Fibrous Silica-Titania (FST) were prepared via microemulsion technique with a different sequence of titania incorporation method. The catalysts were characterized by x-ray diffraction (XRD), N$_2$ adsorption-desorption, field emission scanning electron microscopy (FESEM), transmission electron microscopes (TEM), and fourier-transform infrared spectroscopy (FTIR). The results discovered that the FST catalyst had high crystallinity, higher specific surface area, and large pore volume. The alternate arrangement of TiO$_2$ and silica in the framework of fibrous silica on FST catalyst had an excellent dispersion and it triggered stronger TiO$_2$–SiO$_2$ interactions. It was observed that in the absence of triethylamine (TEA), formic acid (HCOOH) was much favourable produced by both catalysts, with the highest HCOOH product was obtained using TiO$_2$/KCC-1 (2933 μmol/g$_{cat}$.h). In the presence of TEA as a sacrificial agent, superior methanol production was perceived using FST (3487 μmol/g$_{cat}$.h) as compared to TiO$_2$/KCC-1 (2773 μmol/g$_{cat}$.h). It was proposed that the unique structure of the FST catalyst absorbed many photons and was able to absorb more carbon dioxide (CO$_2$) molecules onto the active site of the catalyst to produce carbonic acid (H$_2$CO$_3$) active radicals. With the assist of TEA, methanol production drastically boosts up almost three times higher than the absence of TEA, probably due to an excess of electrons leading to the formation of more active radicals, thus enhancing the methanol production. The response surface methodology (RSM) result indicated that the utmost yield could be obtained at catalyst dosage 0.619 g/L, TEA volume 157.24 μL, and CO$_2$ flow rate 9.47 mL/min. The experimental validation of the predicted optimum condition revealed that the methanol yield is 3062.966 mol g^{-1} h^{-1}, compared to the predicted value of 3026.95 mol g^{-1} h^{-1}, with only a 1.18% difference.

1. Introduction

The rising of atmospheric carbon dioxide (CO$_2$) concentration is gaining prominence nowadays appointed to the unceasing consumption of fossil fuels in satisfying the fast growth of industrial activities, triggering the drastic change of the world's climate like rising of earth's average temperature and sea level [1]. In view of this, researchers from around the world have turned their attention to developing strategies to lessen the CO$_2$ release [2,3]. Recently, the sustainable approach of converting CO$_2$ to methanol (CH$_3$OH) via photocatalytic reduction has been recognized as an enticing route towards lessening CO$_2$ emissions.

In fact, the photoreduction process is particularly advantageous since it can be conducted under relatively mild conditions with lower energy input and requires highly available solar irradiation as energy and water (H$_2$O) as electrons and protons sources [4]. Additionally, the generated CH$_3$OH within this route possessed wide application as a fuel, solvent, or feedstock for further chemical production (e.g. methyl and vinyl acetates, methyl methacrylate, methylamines, and acetic acid) [5].

By considering the thermodynamically stable character of the CO$_2$ molecule and the energetically unfavorable nature of photoreduction pathways, innovative photocatalysts are essential to promote CO$_2$ photoreduction and improve the effectiveness of solar energy

conversion processes. In literature, various semiconductors have been utilized for this work since these metals possessed an ideal band structure capable of assisting the reduction of CO_2 [6–9]. Among the numerous semiconductors utilized in the literature, TiO_2 is frequently employed as a photocatalyst for the CO_2 photoreduction process attributed to its high availability, low toxicity, low cost, and great thermal stability [10]. However, TiO_2 possesses several restrictions for CO_2 photoreduction; (1) has a wide band gap, which lessens solar energy conversion efficiency; (2) has fast photoinduced electron-hole pairs recombination rate, lowering the photocatalytic activity; (3) has limited CO_2 adsorption capacity, which results in poor fuel production rate [10].

Extensive efforts towards TiO_2 modification have been employed in literature to overcome these weaknesses, like the coupling of TiO_2 with porous silica, since this strategy can prevent fast charge recombination rate and improve the dispersion of accessible TiO_2 particles. For example, Yang et al. (2009) experienced a considerable enhancement in photoreduction activity about 3 times after successfully employing Santa Barbara Amorphous-15 (SBA-15) as supported for TiO_2 via sol-gel approach compared to pure TiO_2 [11]. The author claimed that this finding resulted from the improvement in thermal stability of the TiO_2 anatase, enhancement in diffusion and adsorption of reactants, excellent dispersion of TiO_2 particles, and the suppression of TiO_2 crystalline growth.

Lately, the employment of dendrimer-like silica fibrous structures such as KAUST Catalysis Center (KCC-1) and fibrous silica loaded with metal oxide materials has aroused interest among researchers in the photocatalytic field owing to its unique morphology, which provides the increment in the quantity of active sites' accessibility, triggering the improvement in catalytic performance [12–15]. Singh et al. (2016) evaluated and compared the photodegradation of dye using TiO_2 supported with different types of support (KCC-1, SBA-15, and MCM-15). The high and efficient performances as evidenced by the authors for the TiO_2/KCC-1 compared to SBA-15 and MCM-15 credited to; (1) excellent dispersion and great accessibility of active TiO_2 sites, (2) the fibrous structure of KCC-1 led to the increment in the number of incident light reflections, thus enhancing the light-harvesting capability of TiO_2, (3) large surface area which assisting the improvement in adsorption during the reaction [12]. In our previous work, the generation of fibrous silica-titania (FST) via microwave radiation for the photodegradation of ibuprofen proved that the fibrous structure of this material caused the improvement in the number of accessibility active sites, surface defects, and oxygen vacancies, which results in the excellent photocatalytic performance [14].

Thus, it is plausible to utilize these types of materials as photocatalysts for improving the efficiency of CO_2 photoreduction to CH_3OH by considering the dispersion of the TiO_2, capability of light-harvesting, and higher surface area. As far as we are aware, this work reported the first-ever employment of the FST and TiO_2/KCC-1 in CO_2 photoreduction to CH_3OH. The photoreduction performance of these catalysts under visible light irradiation was compared as well as the mechanism for the photoreduction of CO_2 to methanol over both FST and TiO_2/KCC-1 catalysts was proposed within this work.

2. Experimental

2.1. Materials

Toluene, urea, 1-butanol, cetyltrimethylammonium bromide (CTAB), and tetraethyl orthosilicate (TEOS) were purchased from Merck Sdn. Bhd. Triethylamine (TEA) and titania seed (JRC TiO_2) were obtained from Sigma Aldrich. The naphthalene was obtained from Fluka and N, N- Dimethylformamide (DMF) was bought from J. T. Baker. Platinum (Pt) and Titania (Ti) plates were procured from Nilaco, Japan. All chemical were utilised in their natural state, with no treatment. The CO_2 gas with 99% purity was used as the feed gas.

2.2. Synthesis of photocatalysts

Firstly, fibrous silica KCC-1 was prepared using microemulsion technique as described in a literature [16]. In brief, 8 g urea and 12.4 g CTAB were dissolved in distilled water. This solution was then combined with another solution containing 1: 23: 1 molar ratios of TEOS, toluene, and butanol, respectively. The mixture was then vigorously stirred for 2 h to ensure homogeneity before being heated at 403 K. After cooling, the solution was centrifuged, then the solid sediments were dried overnight at 383 K, and calcined at 823 K for 6 h. The as prepared fibrous silica KCC-1 was ready to be use.

Then, the incorporation of TiO_2 onto the KCC-1 (TiO_2/KCC-1) catalyst were synthesized by an electrolysis method [17]. A typical cell with a Pt plate as cathode and a Ti plate as anode containing 1.66 mmol of naphthalene, 0.1 M TEAP, and 1 g KCC-1 was filled with 15 mL of DMF solution. The electrolysis was then carried out under an open-air environment with a constant current density of $120 \, \text{mA cm}^{-2}$ and continuous agitating. Following electrolysis, the catalyst was impregnated, dried overnight at 383 K, and then calcined at 823 K for 3 h.

FST catalysts were synthesized using a same method as preparation of KCC-1 catalyst. [18]. However, the titania seed (JRC TiO_2) was added right before mixing with the solution containing TEOS, toluene, and butanol, rather than using electrolysis. The following step are same as mentioned before.

2.3. Characterization of catalyst

The crystallinity of the catalysts was confirmed using X-ray diffraction (XRD) patterns recorded on a powder diffractometer (Bruker Advance D8). FESEM (JEOL JSM-6701 F) and TEM (Philips EM420) were used to investigate the morphological properties of the catalysts. The nitrogen adsorption-desorption analysis of the samples was analyzed using a Beckman Coulter SA3100 surface area analyzer at 77 K. The catalyst functional groups were studied using FT-IR spectroscopy (Perkin Elmer Spectrum GX FTIR Spectrometer).

2.4. Photoconversion of CO2 to methanol

The photoactivity of the catalysts will be investigated via photoconversion of CO_2 to methanol. The schematic diagram of the reactor was illustrated in Fig. S1. The 0.6 g/L (Fig. S2) of photocatalyst will be dispersed into a 100 μL solution which consists of distilled water and TEA (sacrificial agent). The photocatalytic conversion of CO_2 will be conducted using a fixed batch reactor with a cooling system. CO_2 is fed into the photoreactor through a gas inlet tube at the top. A 39 W metal halide lamp with a wavelength of 400 nm was plugged in for a visible light source. To establish adsorption equilibrium, the solution will be agitated in the dark for 60 min before being exposed to visible light for another 4 h. Then, the concentration of methanol will be analyzed using Gas chromatography (GC).

2.5. RSM studies

A common method for achieving the optimal response within a given range is response surface methodology (RSM). In this work, Central Composite Design (CCD) with Design-Expert software was employed to optimize the CO_2 photoconversion to methanol using FST catalyst. Dosage of catalyst (0.35–0.55 g/L), TEA volume (100–200 μL), and CO_2 flow rate (5–15 mL/min) are among the parameters. The viability of the developed model was assessed using a 5% level of significant variance (ANOVA) analysis, in which the null hypothesis can be rejected as long as the calculated F -value is greater than the tabulated F -value.

3. Results and discussion

3.1. Catalyst characterization

3.1.1. Crystallinity, phase, and structural studies

Fig. 1 depicts the wide-angle XRD patterns of TiO_2/KCC-1 and FST catalysts in the range of $2\theta = 5$–$90°$. A broad peak below $2\theta = 23°$ was observed for both catalysts which attributed to the amorphous silica phase (ICDD No-00–039–1425) [19]. Meanwhile, the existence of TiO_2 was confirmed by the occurrence phase with eight significant diffraction peaks at $2\theta = 25.4$ (101), 37.8 (004), 48.2 (200), 53.9 (105), 55.3° (211), 63.2° (204), 75.1° (215) and 84.0° (303). All of the diffraction peaks are well defined and can be pinpointed to the anatase TiO_2 (ICDDNo-01–071–1166) [14,20]. The anatase $TiO2$ nanoparticles were previously known to be highly photoactive and useful for water treatment and carbon dioxide conversion [21]. The high intensity of those peaks for FST, indicating the higher crystallinity of the catalyst.

3.1.2. Textural studies

N_2 physisorption is considered to be a reliable technique to study the textural properties of catalysts. Fig. 2A represents the isotherms for both TiO_2/KCC-1 and FST catalysts. Both catalysts showed type IV isotherm with H1 hysteresis loop corresponded to the typical isotherm for mesoporous material according to the IUPAC classifications [14,16,22]. The higher N_2 uptake observed on the FST catalyst signifies the higher porosity characteristic possessed by the FST. The presence of two phases at $P/Po = 0.2$–0.4 and 0.9–1.0 was verified the presence of intra and interparticle pores accordingly [23]. The slightly dropped of N_2 adsorption by the TiO_2 loaded on KCC-1 indicating successful embedment of metal oxide TiO_2 support resulted in pore blockage phenomenon [24]. The Barrett-Joyner-Halenda (BJH) analysis method was employed to clarify the pore size distribution of the catalysts and presented in Fig. 2B. It was found that a peak within 4–20 nm of FST was attributed to mesopore. The mesopores formed upon the synthesis from the self-assembly of surfactant into micelles and the spaces between the dendrimeric silica (inter-dendrimeric distance) spontaneously [25]. Meanwhile, these pore sizes decreased for TiO_2/KCC-1 as depicted in Fig. 2B indicating the pore blockage by TiO_2 particles.

The surface area and pore volume for each catalyst was calculated in Table 1. The calculated BET surface area of FST and TiO_2/KCC-1 were 616 and 561 m^2/g respectively. The higher surface area of FST might be attributed to the richness of dendrimeric silica fibers and the absence of pore blockage phenomenon. The lower surface area of TiO_2/KCC-1
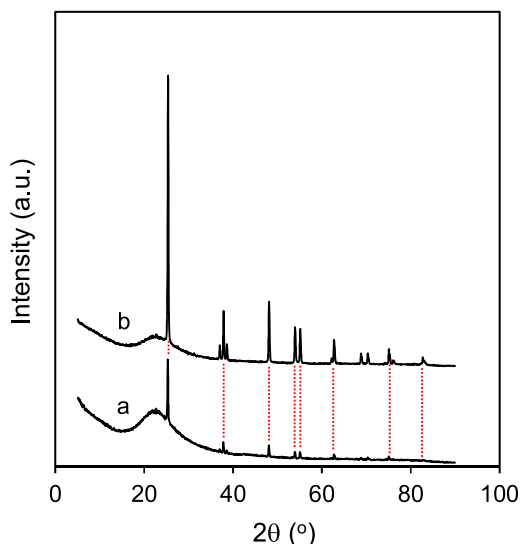
owing to the accumulation of Ti metal oxide on the surface of the catalyst. This postulation could also be because of the partially collapsed catalyst wall upon the embedment of metal oxide cluster associated with the inner surface pores of KCC-1 [26]. Besides, the total pore volume for FST and TiO_2/KCC-1 were 1.54 and 1.26 cm^3/g respectively. This could be further confirmed the blockage of the pore that occurred in TiO_2/KCC-1 resulted in the reduction of the pore volume. These phenomena would help more TiO_2 active species and satisfactory adsorption sites for CO_2 molecules and photons onto the FST catalyst, hence could enhance the photoconversion of CO_2 to methanol.

3.1.3. Vibrational spectroscopy

FT-IR spectroscopy was used to investigate the surface chemistry of TiO_2/KCC-1 and FST in the range 4000 – 400 cm^{-1} as demonstrated in Fig. 3A. Five main bands were observed at 1631, 1083, 964, 798, and 462 cm^{-1}, which are assigned to water molecules retained by siliceous materials, Si-O-Si asymmetric stretching, external Si-OH groups, Si-O-Si symmetric stretching, and Si-O-Si bending vibration, respectively [22, 27]. It could be seen that the FST has lower intensity compared to TiO_2/KCC-1, signifying the alternate arrangement of TiO_2 and silica in the framework of fibrous silica supposed to trigger more interactions between both species [14]. A similar finding was observed for fibrous silica Zn (FSZn) for photocatalytic desulphurization, in which FSZn has less intense bands than ZnO_2/KCC-1 [28]. The deconvoluted band at 964 cm^{-1} (Fig. S3) for both catalysts were summarized in Fig. 3B. The peak was deconvoluted into three possible main bands, assigned to Si–O–Ti interaction (935 cm^{-1}), non-bridging free broken Si–O stretching (948 cm^{-1}) and Si–O–H stretching (967 cm^{-1}). It was observed that the peak at 935 cm^{-1} is highest for FST catalyst proving more formation of Si–O–Ti bonds signified that the titania had been embedded into the silica framework during the synthesis process. The highest number of interactions between TiO_2 and SiO_2 suggesting the generation of an efficient TiO_2–SiO_2 heterojunction in FST. The heterojunction formed between the two composites can promote the separation of e^- and h^+, prevent the charge-carrier recombination, and prolong the lifetime of photocarriers in the photocatalyst, hence, further boost the yield of methanol [29].

3.1.4. Morphological studies

The morphology of as-prepared catalysts was further elucidated by FESEM (Fig. 4). Based on Fig. 4A depicted low magnification, it is seen that the TiO_2/KCC-1 possesses a generally spherical dendritic silica with a small particle dispersed on the outside surface that belongs to TiO_2, which is equivalent to the assembly of KCC-1 that was reported by a previous researcher [30]. Meanwhile, FST (Fig. 4B) shows a similar morphology, however, the particle size is found to be smaller than TiO_2/KCC-1. Additionally, high magnification images indicate that the FST retains a thick layer of dendritic without collapsed a sphere shape compared to TiO_2/KCC-1. This phenomenon was due to titanium sources for FST being successfully loaded alternately in silica. Therefore, FST composed a well-dispersed of Ti and perfectly spherical structure, which could benefit the performance.

This was also in line with TEM images illustrated in Fig. 5 (A-B) and (C-D) for TiO_2/KCC-1 and FST, respectively. In specific, Fig. 5B displays a TEM image for TiO_2/KCC-1 with the Fast Fourier transform (FFT) patterns (insert figure), which further confirmed the presence of TiO_2 nanoparticles on the KCC-1 particularly dispersed at the outer surface of the dendrimeric silica. As shown by the FFT patterns in Fig. 5D, magnification on darker area of the fibrous tips confirmed the crystalline with D-spacing of 0.35 nm, elucidating the (1 0 1) lattice of anatase phase TiO_2. Identical D-spacing of the TiO_2 anatase phase was also determined by previous work [31]. Furthermore, it could be claimed that the structure of FST dendrimeric fibres was formed alternately with amorphous SiO_2 and anatase TiO_2. This unusual arrangement is thought to benefit the photoconversion of CO_2 to methanol.
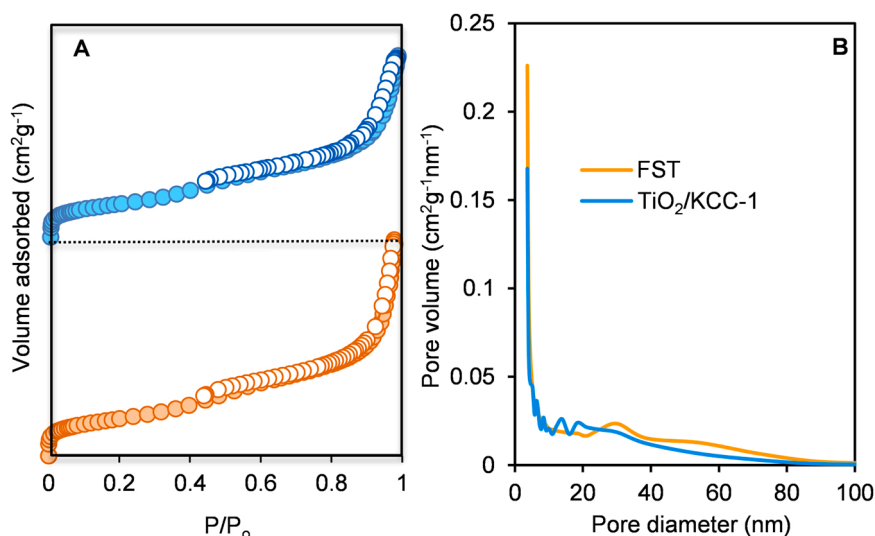

Fig. 1. XRD diffractogram for (a) TiO2/KCC-1 and (b) FST catalysts.

Fig. 2. N_2 adsorption-desorption.

Table 1
Textural properties of all catalysts.

Catalyst	Surface area (m^2/g)	Total Pore volume (cm^3/g)	Band gap (eV)	Methanol Yield[a] $(\mu molg^{-1}h^{-1})$
$TiO_2/$ KCC-1	561	1.26	3.10	2773
FST	616	1.54	2.82	3487

[a] The CO_2 was convert to methanol in the presence of trimethylamine.

3.2. Photocatalytic performance

Fig. 6 and Fig. 7 represents the photocatalytic conversion of CO_2 over TiO_2/KCC-1 and FST catalysts under visible light. The photocatalytic reaction was performed in two conditions, which are without and with the presence of a triethylamine (TEA) sacrificial agent. It was observed that in the absence of triethylamine (TEA), formic acid (HCOOH) was favourable produced by both catalysts, with the highest HCOOH product was obtained using TiO_2/KCC-1 (2933 $\mu mol/g_{cat}$.h). After the addition of TEA, a superior methanol production was perceived using FST (3487 $\mu mol/g_{cat}$.h), as compared to TiO_2/KCC-1 (2773 $\mu mol/g_{cat}$.h).

The best CO_2 photoconversion of FST to the desired methanol product was most probably due to the role of TEA as a sacrificial electron donor that offers a surplus of electrons for the formation of additional active radicals, thus enhanced photocatalytic reaction [32]. This improved performance also was resulted from the well-dispersion nature of TiO_2 species which were alternated with dendrimeric silica fibrous, higher specific surface area and pore volume, stronger interaction between TiO_2 and SiO_2, as well as an appropriate band gap energy (Table 1) of FST [14]. It is worth mentioning that the well-dispersion behavior of TiO_2 together with the existence of high surface area and large pore volume of FST have provided an adequate TiO_2 active species and satisfactory adsorption sites for CO_2 molecules and photons, respectively [33]. Meanwhile, the presence of a stronger TiO_2 and SiO_2 interaction and a suitable band gap position hinting the generation of an efficient TiO_2–SiO_2 heterojunction in FST with a fruitful formation of different active radicals [34]. Undoubtedly, all these beneficial criteria assisted by TEA addition have synergistically enhanced the CO_2 photoconversion to methanol in terms of high photoactivity and selectivity.

For evaluation, an additional experiment of photoconversion of CO_2 to methanol was also conducted by using TiO_2 commercial at the same condition to compare its performance towards the synthesized catalyst.
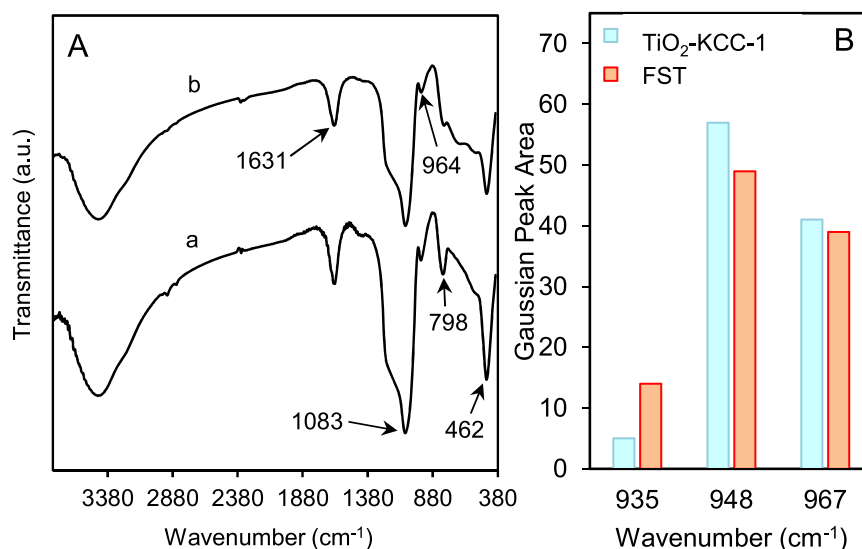

Fig. 3. A) FTIR spectra for (a) TiO_2/KCC-1 and (b) FST catalysts B) deconvolution at peak 964 cm^{-1} for TiO_2-KCC-1 and FST.
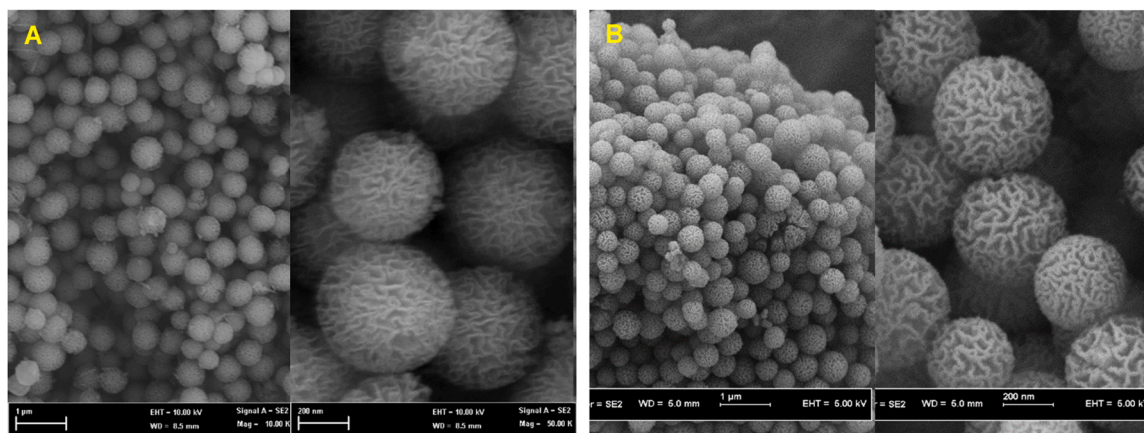
Fig. 4. FESEM images for (a) TiO$_2$/KCC-1 and (b) FST catalysts with different magnification.
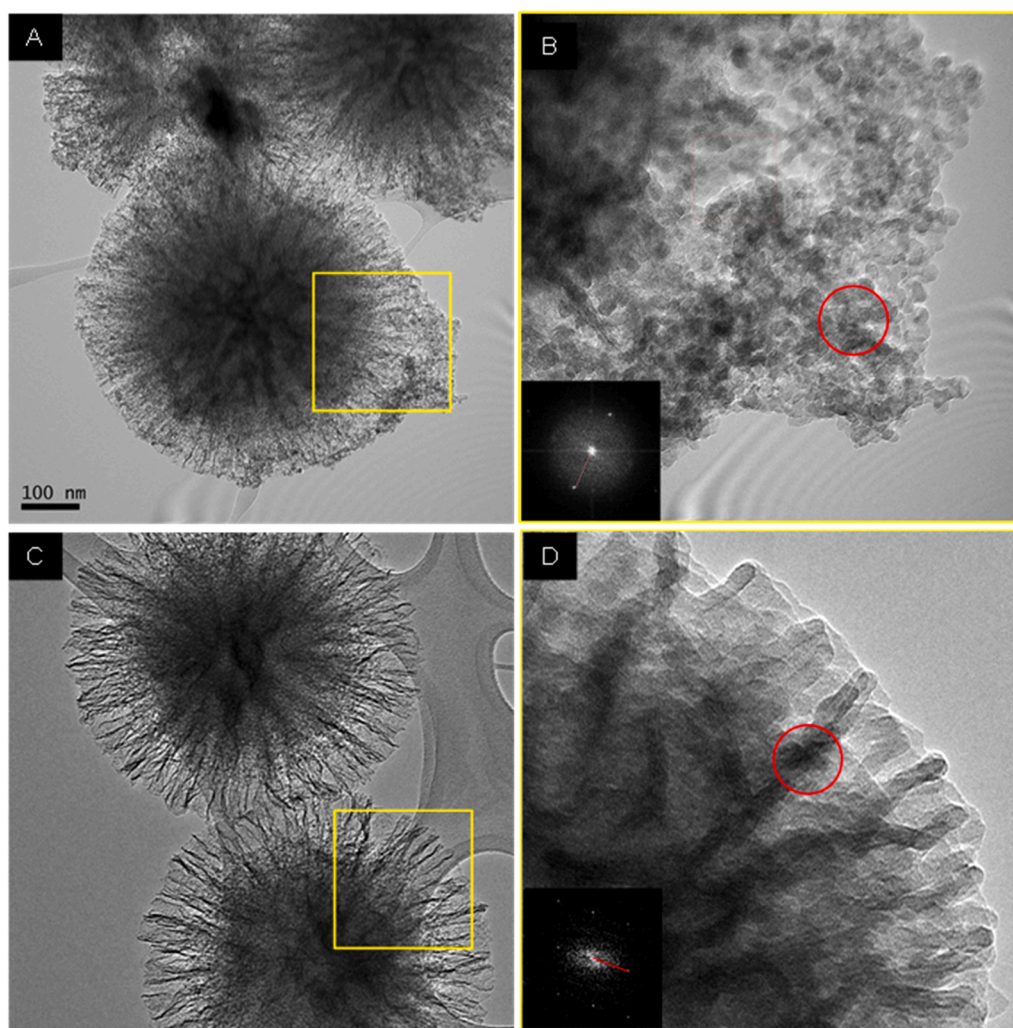

Fig. 5. TEM image of (A and B) TiO$_2$/KCC-1, (C and D) FST with insert figure are its corresponding FFT.

As shown in Fig. S4, in the presence of TEA, the methanol yield obtained by commercial TiO$_2$ was only 842 µmol/g$_{cat}$.h and it was lower than both FST and TiO$_2$-KCC-1. Moreover, it was also observed that commercial TiO$_2$ produced more HCOOH rather than methanol proving that the modification of TiO$_2$ gave significant effect on the methanol production.

3.3. Proposed reaction mechanism

The reaction was carried out at pH 5 where bubbling of CO$_2$ in water at this condition led to the formation of carbonic acid (H$_2$CO$_3$) as shown in Eq. 1 [35,36].

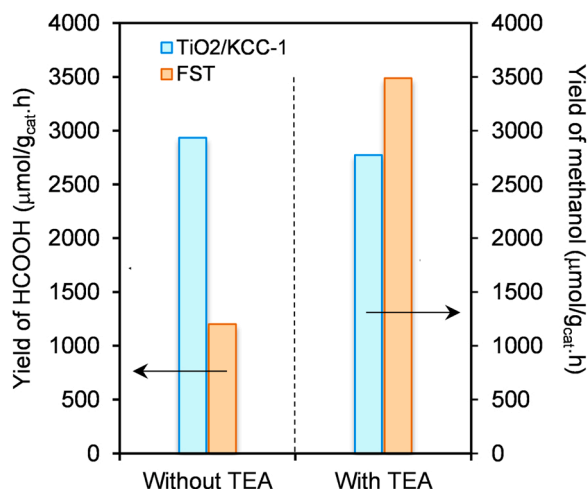$$CO_2 + H_2O \Leftrightarrow^{pH \ 5} H_2CO_3 \tag{1}$$

Fig. 6. Effect of TEA as a sacrificial agent in CO_2 reduction over both catalysts [CO_2 (10 mL/min), 0.6 g/L catalyst, 100 µL TEA, 60 min].

Light irradiation on photocatalyst excited the electron (e^-) to the conduction band (CB) while leaving the hole (h^+) at the valence band (VB). It was described that the band gap energy for tailored FST was 2.83 eV with the CB and VB at -0.08 eV and 2.9 eV, respectively [14, 22]. In fact, the structure of FST exists alternatingly between dendrimeric fibers of TiO_2–SiO_2 with rich TiO_2 particles at the core of the FST. Therefore, the resulted bandgap position of FST restricted the production of CH_3OH via the CO_2 reduction route. However, the presence of minute TiO_2 species on the surface of FST may explain the formation of 1200 µmol g_{cat}^{-1} h^{-1} HCOOH in the absence of the TEA system which

originated from H_2CO_3 (Eq. 2).

$$H_2CO_3 + \quad 2H^+ + 2e^- \rightarrow HCOOH + \quad H_2O \qquad (2)$$
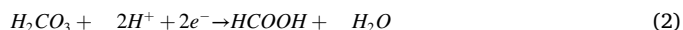
With the assist of TEA as electron donor, the production of CH_3OH boosted up drastically with almost three times higher compared to the without TEA system which assuredly the unique structure of FST offers larger active sites and accelerated the rate of CH_3OH production (route not shown). Furthermore, TEA itself not only worked as an electron donor but also can produce CO_2 in the presence of visible light in the reaction medium, which can accept 6 e^- and 6 H^+ to produce methanol as well, thus could help in enhancing the yield of methanol [37].

In contrast, the ensued band gap energy of TiO_2/KCC-1 catalyst seems not in the desired range at all, thus the well-dispersed TiO_2 particles on the surface of KCC-1 undoubtedly being the main factor in leading the oxidation of water at VB to reduce the H_2CO_3 to HCOOH at the CB. In the presence of TEA, 2773 µmol $gcat^{-1}$ h^{-1} yield of CH_3OH was obtained which supposed to produce via both following routes,

$$H_2CO_3 + \quad 6H^+ + 6e^- \rightarrow CH_3OH + \quad 2H_2O \qquad (3)$$

$$CO_2 + \quad 6H^+ + 6e^- \rightarrow CH_3OH + \quad 2H_2O \qquad (4)$$

A similar amount of active sites from TiO_2 particles maybe give a similar yield of HCOOH and CH_3OH in the absence and presence of TEA, respectively. By the way, the formation of formaldehyde (HCHO) most probably is too rapid to be detected during the reaction.

3.4. Optimization by response surface methodology

The central composite design (CCD) was used to design all 16 experiments, and the results are shown in Table S1. In this study, three parameters were investigated: X_1: catalyst dosage, X_2: TEA volume, and
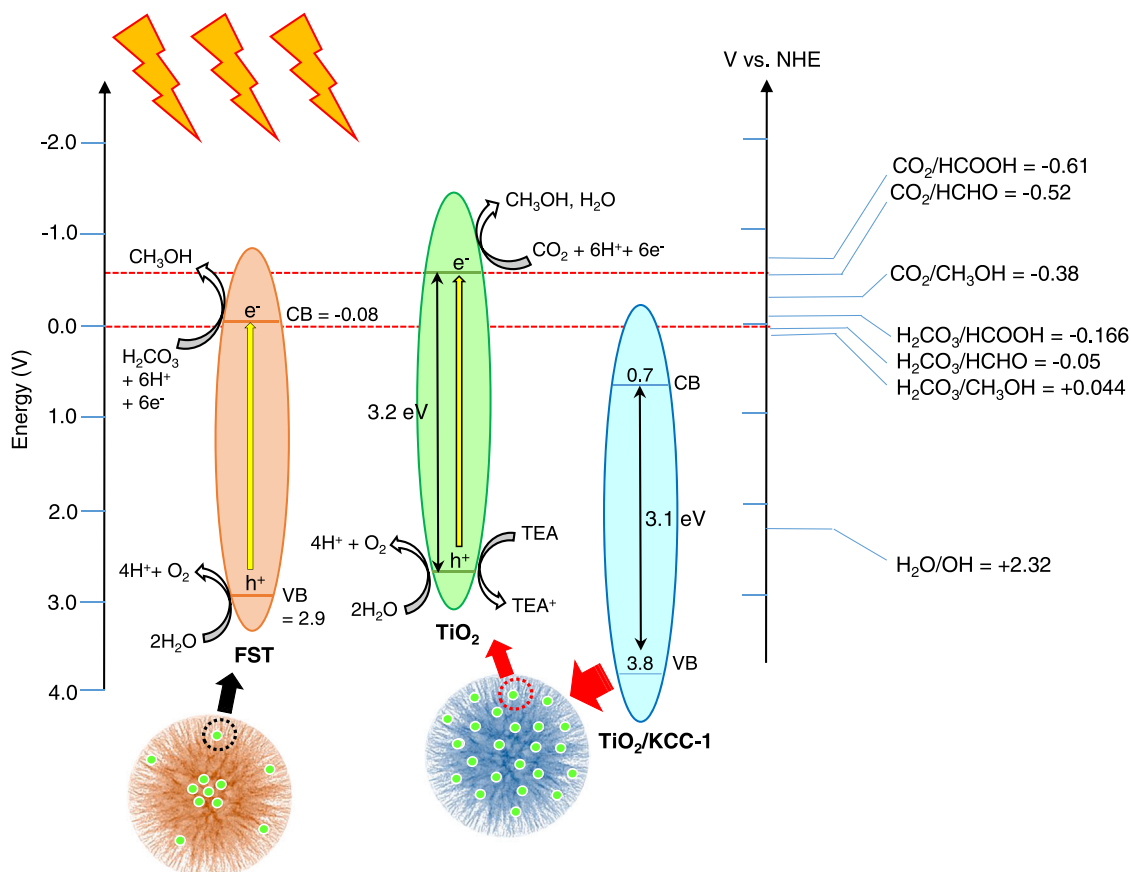

Fig. 7. Proposed mechanism of CO_2 conversion to methanol over FST and TiO_2/KCC-1 catalysts.

X_3: CO$_2$ flowrate. Based on the RSM result, the obtained data were matched into the general quadratic polynomial (Eq. 5) and the final model was stated as in Eq.6:

$$y = \beta_0 + \sum_{i=1}^{k} \beta_i + \sum_{i=1}^{k} \beta_{ii} x_i^i + \sum \sum_{i=1}^{k} \beta_{ij} x_{ij} x_{ij} + \varepsilon \quad (5)$$

where y is the calculated response, ß$_0$ is the intercept term, ß$_i$, ß$_{ij}$ and ß$_{ii}$ are the measure of the effect of variable x$_i$, x$_i$x$_j$, and x$_i$^{2}, respectively and ε is the residual associated to the experiments [38].

$$Y = 3009.52 + 60.8X_1 + 401.20X_2 - 73.2X_3 - 644.55X_1^2 - 1436.55X_2^2$$
$$- 368.53X_3^2 + 154.75X_1X_2 + 15.25X_1X_3 + 14.9X_2X_3 \quad (6)$$

As shown in Fig. 8 A, the projected values were plotted against the experimental values obtained from the photoconversion experiments. The linear regression coefficient, R^2, was found to be close to 1, indicating that the model was correct and significant. The ANOVA analysis of CO$_2$ photoconversion to methanol using FST catalyst is presented in Table 2. According to the ANOVA results, the model was significant, as evidenced by a larger calculated F -value (F-model = 38.099) than a tabulated F -value (Ftable = 4.099) for the respective degree of freedom and probability (p = 0.05).

The t-distribution values in a Pareto chart, as well as the related p-values of the variables for the CO$_2$ photoconversion to methanol using FST, are shown in Fig. 8B. The relevance of the related parameter was determined using the p-value and t-value values, with the smaller p-value and bigger figure of the t-value representing the more vital parameter. From the analysis, both quadratic and linear terms of TEA volume and quadratic terms of catalyst dosage are statistically significant owing to the p-value < 0.05. It is noted that the quadratic effects of TEA volume (X$_2$^{2}) stand up as the most crucial parameter of the regression model and this result is in line with the analysis of variance (ANOVA) as presented in Table 2 which is evidence that quadratic terms of TEA volume as the most significant factor with a value of 1 360 153 for CO$_2$ photoconversion. This can be explained as the availability of active sites depending on the number of TEA as a sacrificial agent in the solution. TEA as an electron donor would boost up the formation of CH$_3$OH species directly from CO$_2$ and H$_2$CO$_3$ species due to sufficient electrons in the solution. Thus, it could enhance the photoconversion of CO$_2$ to methanol. This finding match with the experimental data where the presence of TEA accelerates the production of CH$_3$OH. This is also in good agreement with previous observations, that increasing the TEA volume favors the rich electron donors leading to the conversion of CO$_2$ or HCO$_3$ directly to methanol, finally leading to higher methanol yield [39,40].

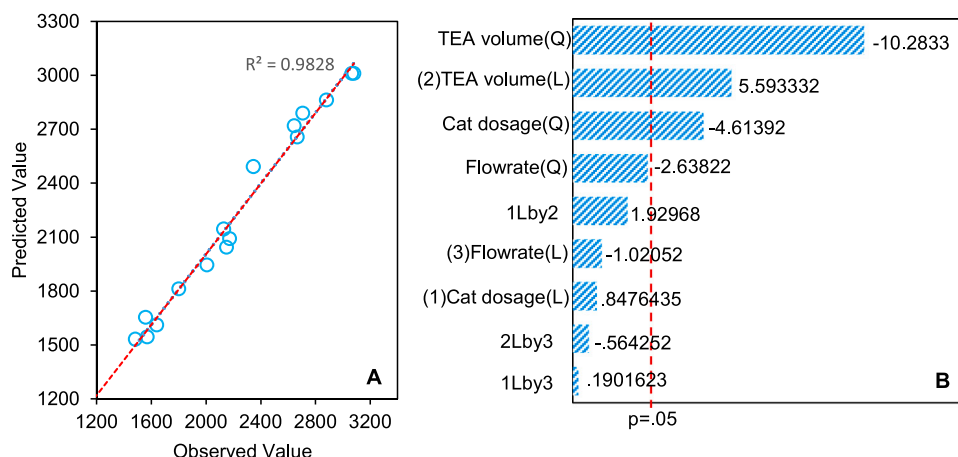Simple approaches for studying and optimising the efficiency of the

Table 2
Analysis of variance (ANOVA) for the yield of methanol.

Factor	Sum of squares (SS)	Degree of freedom (df)	Mean square (MS)	F-value	p-value
Model	4410330	9	490036.7	38.099	
(1) Catalyst dosage (L)	9242	1	9242	0.7185	0.429147
Catalyst dosage (Q)	273817	1	273817	21.2883	0.003638
(2) TEA volume (L)	402404	1	402404	31.2854	0.001389
TEA volume (Q)	1360153	1	1360153	105.7468	0.000049
(3) Flowrate (L)	13396	1	13396	1.0415	0.346855
Flowrate (Q)	89525	1	89525	6.9602	0.038632
1 L by 2 L	47895	1	47895	3.7237	0.101889
1 L by 3 L	465	1	465	0.0362	0.855453
2 L by 3 L	4095	1	4095	0.3184	0.593032
Residual	77174	6	12862		
Total SS	4487504	15			

reaction process include response surfaces and contour graphs. To better understand the relationship between methanol yield and studied variables X$_1$, X$_2$, and X$_3$, three-dimensional surface graphs based on polynomial functions were plotted. Fig. 9 (A) displays the relationship between TEA volume and catalyst dosage, while Fig. 9 (B) and 9 (C) correspond to flow rate and TEA volume, flow rate, and catalyst dosage, respectively. All of the response surface plots had an elliptical shape, indicating a good interaction between the variables studied. [41].

Fig. 9 A presents the 3D surface plot showing the effect of catalyst dosage (X$_1$) and TEA volume (X$_2$) on the methanol yield onto the FST catalyst. It was observed that the yield of methanol increased at the catalyst dosage range of 0.2–0.5 g/L and TEA volume of 80–170 μL. However, the methanol yield decreased with the increase in both catalyst dosage (>0.5 g/L) and TEA volume (>170 μL). It can be ascribed to an excess of catalyst in the solution, which restricts light irradiation and impedes photoconversion. On the other hand, there is also tends to the accumulation of reaction products on the photocatalyst surface. These phenomena would decrease the efficiency of the photoconversion of CO$_2$.

The relationship between CO$_2$ flow rate and TEA volume on methanol yield was displayed in Fig. 9B. The result shows that the CO$_2$ flow rate gave not much a significant effect on methanol yield at the low amount of TEA volume (80 μL), but the yield increased upon increasing TEA volume up to 160 μL and decreased when more amount of TEA volume was added. This finding was matched with the analysis of
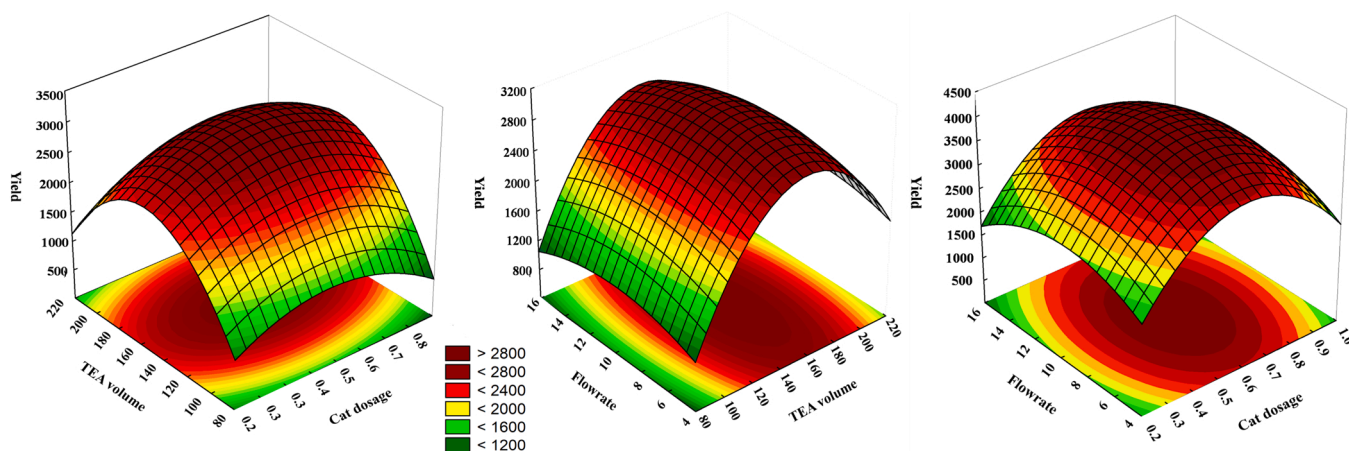

Fig. 8. (A) Predicted vs. observed value plot of the model and (B) Pareto chart of the standardized effect estimate.

Fig. 9. Response surface plots of the combined (A) TEA volume and catalysts dosage (B) flowrate and TEA volume and (C) flowrate and catalyst dosage.

variance (ANOVA) in Table 2 and Pareto chart in Fig. 8B which the mean square value (4095) and t-value (−0.564) for 2 L by 3 L was lower compared to other variables, supporting that the relationship of these variables had a less significant factor for methanol production. As mentioned before, there is a tendency of the coverage of reaction products on the photocatalyst upon increasing TEA volume. The addition of CO_2 flowrate would not give a significant effect due to the coverage of the reaction product having diminished the adsorption of CO_2 on the active site of the catalyst, hence suppressing the production of methanol.

Fig. 9 C shows the relationship of CO_2 flow rate and catalyst dosage on methanol yield. The results show increasing catalyst dosage up to 0.7 g/L and flow rate up to 10 mL/min will increase the yield of methanol. In contrast, further addition of catalyst dosage more than 0.7 g/L and 10 mL/min of CO_2 flow rate will decrease the yield of methanol. This is probably due to the high CO_2 flow rate would lower the adsorption process onto the active site of the catalyst as well as the surplus amount of catalyst used blocked the light penetration hence hindering the photoconversion reaction.

The optimization result revealed that the highest yield was possible at the catalyst dosage 0.619 g/L (X_1), TEA volume 157.24 μL (X_2), and CO_2 flow rate 9.47 mL/min (X_3). Verification experiments performed at the predicted conditions derived from analysis RSM demonstrated that the experimental (3062.966 μmol/g h^{-1}) values were reasonably close to the predicted values (3026.95 μmol/g h^{-1}) with only 1.18% difference. This confirms the validity and adequacy of the predicted models. The error considers small as the value is still below the 10% level of significance.

3.5. Comparison study

Table 3 shows the photocatalytic CO_2 reduction performance of various semiconductor photocatalysts. It can be found that FST exhibits higher photocatalytic CO_2 conversion to methanol activities compared with most of the recently reported photocatalysts. Few based semiconductor photocatalysts were modified with metals such as Cu, Zn, Au, Pt, and Ni which increased the cost and restricted the large-scale usage [42–46]. The non-metal cocatalyst such as carbon-based photocatalyst (rGO and MWCNT) can be of great interest for the conversion of CO_2 to methanol [47,48]. There are several sacrificial agents for the aforementioned works such as isopropanol, TEOA, Na_2SO_3 and TEA. For confirmation, prior experiments were done on the effect of sacrificial agent and the results were tabulated in Table S2. It was observed that TEA gave the best performance on methanol production. Based on the result, TEA was selected as sacrifial agent for the present study owing to the its high oxidation potential. Nevertheless, despite the efficient

Table 3
Comparisons of CO_2 conversion to methanol using TiO_2-based catalysts.

Photocatalyst	Light sources	S_{BET} (m^2/g)	Sacrificial agent	Methanol Production (μmol g^{-1} h^{-1})	References
CuO-NaTaO$_3$	Visible	–	Isopropanol	1302.22	[42]
ZnO/ZnSe	UV	–	Isopropanol	1581.82	[43]
NiO-KTaO$_3$	UV	–	Isopropanol	1815	[44]
Au/TiO$_2$	UV	55	Na$_2$SO$_3$	1360	[45]
Ni$_2$P/CdS	Visible	–	TEA	2843	[46]
Pt/TiO$_2$	Visible	–	TEA	1424.8	[46]
MWCNT/ TiO$_2$	UV	427	TEOA	3246.1	[47]
rGO-TiO$_2$	UV	115.2	TEOA	2330	[48]
TiO$_2$/KCC-1	Visible	561	TEA	2773	Present study
FST	Visible	616	TEA	3487	Present study

rGO: reduced graphene oxide MWCNT: multiwalled carbon nanotubes.

performance for the production of methanol, the utilization of UV light as an irradiation source was not favored in the industrial application as higher photon energy is needed compared to a visible light source. The unique fibrous silica morphology and well dispersion of TiO_2 of the present work seem beneficial for achieving a high yield of methanol. In addition, the great improvement of methanol production could be illustrated due to higher external surface area which offers more space for the reaction to occur effectively. Ideally, this photocatalyst is deemed as a sustainable and promising solution for industrial implementation of the large-scale production of methanol via photocatalytic reduction of CO_2.

4. Conclusion

In this study, titania-supported fibrous silica (TiO_2-KCC1) and fibrous silica-titania (FST) were studied in detail on their properties and performance towards photoconversion of CO_2 to methanol. From XRD and N_2 adsorption-desorption analysis, the FST catalyst had high crystallinity, higher specific surface area, and large pore volume. FESEM image clearly showed the TiO_2/KCC-1 had spherical dendritic silica with a small TiO_2 particle dispersed on the outside surface. Meanwhile, the particle size of TiO_2 was well dispersed on the FST catalyst is found to be smaller than TiO_2/KCC-1. TEM image elucidated the alternate arrangement of TiO_2 and silica in the framework of fibrous silica on FST catalyst and triggered stronger TiO_2–SiO_2 interactions. It was observed that in the absence of TEA, only HCOOH was produced by both catalysts, with the highest HCOOH product was obtained using TiO_2/KCC-1

(2933 μmol/g$_{cat}$.h). In the presence of TEA as a sacrificial agent, superior methanol production was perceived using FST (3487 μmol/g$_{cat}$.h) as compared to TiO$_2$/KCC-1 (2773 μmol/g$_{cat}$.h). It was proposed that the unique structure of the FST catalyst had offered high absorption of photons and adsorptions CO$_2$ molecules onto the active site of the catalyst to produce H$_2$CO$_3$. With the assist of TEA, it offered an excess electron for the formation of active radicals, thus enhancing the methanol production. The optimization result showed that maximum yield could be achieved at catalyst dosage 0.619 g/L (X$_1$), TEA volume 157.24 μL (X$_2$), and CO$_2$ flow rate 9.47 mL/min (X$_3$). Experimental verification of the predicted optimum condition demonstrated that the methanol yield is 3062.966 μmol/g h^{-1} compared to the predicted value of 3026.95 μmol/g h^{-1} with only a 1.18% difference.

CRediT authorship contribution statement

N.F. Khusnun: Writing – original draft, Conceptualization, Methodology, Visualization, Project administration **A.A. Jalil:** Writing – original draft, Conceptualization, Visualization, Supervision, Project administration, Funding acquisition. **T.A.T. Abdullah:** Conceptualization, Supervision, Resources. **S.S.M. Latip:** Methodology, Formal analysis, Investigation, Visualization. **C.N.C. Hitam:** Writing – original draft, Methodology, Investigation, Visualization. **A.A. Fauzi:** Writing – original draft, Formal analysis, Investigation. **N.S. Hassan:** Writing – original draft, Conceptualization, Investigation. **M.A.H. Aziz:** Writing – original draft, Formal analysis, Investigation. **A.F.A. Rahman:** Writing – original draft, Formal analysis, Investigation. **F.F.A. Aziz:** Writing – original draft, Formal analysis **M. Bahari:** Writing – original draft, Visualization. **R.H. Adnan:** Supervision, Project administration. **R. Saravanan:** Writing – review & editing.

Declaration of Competing Interest

The authors declare that they have no known competing financial interests or personal relationships that could have appeared to influence the work reported in this paper.

Acknowledgment

Appendix A. Supporting information

Supplementary data associated with this article can be found in the online version at doi:10.1016/j.jcou.2022.101901.

References

[1] N. Muradov, Low to near-zero CO$_2$ production of hydrogen from fossil fuels: status and perspectives, Int. J. Hydrog. Energy 42 (20) (2017) 14058–14088.

[2] F. Johnsson, Perspectives on CO$_2$ capture and storage, Greenh. Gases: Sci. Technol. 1 (2) (2011) 119–133.

[3] A. Dindi, D.V. Quang, L.F. Vega, E. Nashef, M.R.M. Abu-Zahra, Applications of fly ash for CO$_2$ capture, utilization, and storage, J. CO2 Util. 29 (2019) 82–102.

[4] W.H. Lee, C.H. Liao, M.F. Tsai, C.W. Huang, J.C.S. Wu, A novel twin reactor for CO$_2$ photoreduction to mimic artificial photosynthesis, Appl. Catal. B: Environ. 132 133 (2013) 445–451.

[5] F. Dalena, A. Senatore, A. Marino, A. Gordano, M. Basile, A. Basile, Methanol production and applications: an overview, Methanol.: Sci. Eng. (2018) 3–28.

[6] M.A. Ávila-López, S. Gavrielides, X. Luo, A.E. Ojoajogwu, J.Z.Y. Tan, E. Luévano-Hipólito, L.M. Torres-Martínez, M.M. Maroto-Valer, Comparative study of CO$_2$ photoreduction using different conformations of CuO photocatalyst: powder, coating on mesh and thin film, J. CO2 Util. 50 (2021), 101588.

[7] W. Qingli, Z. Zhaoguo, C. Xudong, H. Zhengfeng, D. Peimei, C. Yi, Z. Xiwen, Photoreduction of CO$_2$ using black TiO2 films under solar light, J. CO2 Util. 12 (2015) 7–11.

[8] J. Núñez, V.A. de la Peña O'Shea, P. Jana, J.M. Coronado, D.P. Serrano, Effect of copper on the performance of ZnO and ZnO1−xNx oxides as CO$_2$ photoreduction catalysts, Catal. Today 209 (2013) 21–27.

[9] R.A. Geioushy, S.M. El-Sheikh, I.M. Hegazy, A. Shawky, S. El-Sherbiny, A.-H. T. Kandil, Insights into two-dimensional MoS2 sheets for enhanced CO$_2$ photoreduction to C1 and C2 hydrocarbon products, Mater. Res. Bull. 118 (2019), 110499.

[10] H. Zhao, F. Pan, Y. Li, A review on the effects of TiO2 surface point defects on CO$_2$ photoreduction with H2O, J. Mater. 3 (1) (2017) 17–32.

[11] H.-C. Yang, H.-Y. Lin, Y.-S. Chien, J.C.-S. Wu, H.-H. Wu, Mesoporous TiO2/SBA-15, and Cu/TiO2/SBA-15 composite photocatalysts for photoreduction of CO$_2$ to methanol, Catal. Lett. 131 (3) (2009) 381–387.

[12] R. Singh, R. Bapat, L. Qin, H. Feng, V. Polshettiwar, Atomic layer deposited (ALD) TiO$_2$ on fibrous nano-silica (KCC-1) for photocatalysis: nanoparticle formation and size quantization effect, ACS Catal. 6 (5) (2016) 2770–2784.

[13] M. Zhang, M. Zhao, R. Chen, J. Liu, Q. Liu, J. Yu, R. Li, P. Liu, J. Wang, Fabrication of the pod-like KCC-1/TiO2 superhydrophobic surface on AZ31 Mg alloy with stability and photocatalytic property, Appl. Surf. Sci. 499 (2020), 143933.

[14] A.A. Fauzi, A.A. Jalil, M. Mohamed, S. Triwahyono, N.W.C. Jusoh, A.F.A. Rahman, F.F.A. Aziz, N.S. Hassan, N.F. Khusnun, H. Tanaka, Altering fiber density of cockscomb-like fibrous silica–titania catalysts for enhanced photodegradation of ibuprofen, J. Environ. Manag. 227 (2018) 34–43.

[15] F. Aziz, A. Jalil, N. Hassan, C. Hitam, A. Rahman, A. Fauzi, Enhanced visible-light driven multi-photoredox Cr (VI) and p-cresol by Si and Zr interplay in fibrous silica-zirconia, J. Hazard. Mater. 401 (2021), 123277.

[16] M.Y.S. Hamid, M.L. Firmansyah, S. Triwahyono, A.A. Jalil, R.R. Mukti, E. Febriyanti, V. Suendo, H.D. Setiabudi, M. Mohamed, W. Nabgan, Oxygen vacancy-rich mesoporous silica KCC-1 for CO$_2$ methanation, Appl. Catal. A: Gen. 532 (2017) 86–94.

[17] N. Khusnun, A. Jalil, S. Triwahyono, N. Jusoh, A. Johari, K. Kidam, Interaction between copper and carbon nanotubes triggers their mutual role in the enhanced photodegradation of p-chloroaniline, Phys. Chem. Chem. Phys. 18 (17) (2016) 12323–12331.

[18] M.L. Firmansyah, A.A. Jalil, S. Triwahyono, H. Hamdan, M.M. Salleh, W.F. W. Ahmad, G.T.M. Kadja, Synthesis and characterization of fibrous silica ZSM-5 for cumene hydrocracking, Catal. Sci. Technol. 6 (13) (2016) 5178–5182.

[19] N.S. Hassan, A.A. Jalil, F.F.A. Aziz, M.A.H. Aziz, I. Hussain, M.W. Ali, New insight into sequential of silica-zirconia precursors in stabilizing silica-doped tetragonal zirconia nanoparticles for enhanced photoactivity, Mater. Lett. 291 (2021), 129582.

[20] N. Sudhakar, R.K. Singh, S.K. Mishra, S. Kannan, Quantitative studies on the size induced anatase to rutile phase transformation in TiO2–SiO2 binary oxides during heat treatments, RSC Adv. 4 (91) (2014) 49752–49761.

[21] S.A. Rawool, K.K. Yadav, V. Polshettiwar, Defective TiO2 for photocatalytic CO$_2$ conversion to fuels and chemicals, Chem. Sci. 12 (12) (2021) 4267–4299.

[22] M.S. Azami, A.A. Jalil, C.N.C. Hitam, N.S. Hassan, C.R. Mamat, R.H. Adnan, N. Chanlek, Tuning of the electronic band structure of fibrous silica titania with g-C3N4 for efficient Z-scheme photocatalytic activity, Appl. Surf. Sci. 512 (2020), 145744.

[23] M.A.A. Aziz, A.A. Jalil, S. Triwahyono, S.M. Sidik, Methanation of carbon dioxide on metal-promoted mesostructured silica nanoparticles, Appl. Catal. A: Gen. 486 (2014) 115–122.

[24] F.F.A. Aziz, A.A. Jalil, N.S. Hassan, A.A. Fauzi, M.S. Azami, Simultaneous photocatalytic reduction of hexavalent chromium and oxidation of p-cresol over AgO decorated on fibrous silica zirconia, Environ. Pollut. 285 (2021), 117490.

[25] M.A.H. Aziz, A.A. Jalil, T.J. Siang, I. Hussain, A.F.A. Rahman, H. Hamdan, Abundant Lewis acidic sites of peculiar fibrous silica zeolite X enhanced toluene conversion in side chain toluene methylation, Fuel 305 (2021) 121432.

[26] K.M. Parida, S. Mallick, P.C. Sahoo, S.K. Rana, A facile method for synthesis of amine-functionalized mesoporous zirconia and its catalytic evaluation in Knoevenagel condensation, Appl. Catal. A: Gen. 381 (1) (2010) 226–232.

[27] A. abdul rahman, A. Abdul Jalil, S. Triwahyono, A. Ripin, F.F.A. Aziz, N.A.A. Fatah, N. Jaafar, C.K. Che Ku Hitam, N.F. Salleh, N. Hassan, Strategies for introducing titania onto mesostructured silica nanoparticles targeting enhanced photocatalytic activity of visible-light-responsive Ti-MSN catalysts, J. Clean. Prod. 143 (2016).

[28] C.N.C. Hitam, A.A. Jalil, Y.O. Raji, Fabrication of fibrous silica zinc (FSZn) composite for enhanced photocatalytic desulphurization, Top. Catal. 63 (11–14) (2020) 1169–1181.

[29] N.S. Hassan, A.A. Jalil, N.F. Khusnun, M.W. Ali, S. Haron, Role of reduced graphene oxide in improving interfacial charge transfer of hybridized rGO/silica/ zirconia for enhanced Bisphenol A photodegradation, J. Alloy. Compd. 789 (2019) 221–230.

[30] V. Polshettiwar, D. Cha, X. Zhang, J.M. Basset, High-surface-area silica nanospheres (KCC-1) with a fibrous morphology, Angew. Chem. Int. Ed. 49 (50) (2010) 9652–9656.

[31] C. Li, T. Sun, D. Zhang, X. Zhang, Y. Qian, Y. Zhang, X. Lin, J. Liu, L. Zhu, X. Wang, Z. Shi, Q. Lin, Fabrication of ternary Ag/La-black TiO2−x photocatalyst with enhanced visible-light photocatalytic activity for tetracycline degradation, J. Alloy. Compd. 891 (2022), 161960.

[32] P.K. Prajapati, H. Singh, R. Yadav, A.K. Sinha, S. Szunerits, R. Boukherroub, S. L. Jain, Core-shell Ni/NiO grafted cobalt (II) complex: an efficient inorganic nanocomposite for photocatalytic reduction of CO$_2$ under visible light irradiation, Appl. Surf. Sci. 467–468 (2019) 370–381.

[33] C.N.C. Hitam, A.A. Jalil, Recent advances on nanocellulose biomaterials for environmental health photoremediation: an overview, Environ. Res. 204 (2022), 111964.

[34] C.N.C. Hitam, A.A. Jalil, S.M. Izan, M.S. Azami, M.H. Hassim, N. Chanlek, The unforeseen relationship of Fe2O3 and ZnO on fibrous silica KCC-1 catalyst for fabricated Z-scheme extractive-photooxidative desulphurization, Powder Technol. 375 (2020) 397–408.

[35] H. Abdullah, M.R. Khan, M. Pudukudy, Z. Yaakob, N.A. Ismail, CeO2-TiO2 as a visible light active catalyst for the photoreduction of CO_2 to methanol, J. Rare Earths 33 (11) (2015) 1155–1161.

[36] K. Li, X. An, K.H. Park, M. Khraisheh, J. Tang, A critical review of CO_2 photoconversion: catalysts and reactors, Catal. Today 224 (2014) 3–12.

[37] B. Duan, L. Mei, A. Z-scheme, Fe2O3/g-C3N4 heterojunction for carbon dioxide to hydrocarbon fuel under visible illuminance, J. Colloid Interface Sci. 575 (2020) 265–273.

[38] M.O. Saeed, K. Azizli, M.H. Isa, M.J.K. Bashir, Application of CCD in RSM to obtain optimize treatment of POME using Fenton oxidation process, J. Water Process Eng. 8 (2015) e7–e16.

[39] Y. Izumi, Recent Advances (2012–2015) in the Photocatalytic Conversion of Carbon Dioxide to Fuels Using Solar Energy: Feasibilty for a New Energy. Advances in CO_2 Capture, Sequestration, and Conversion, American Chemical Society, 2015, pp. 1–46.

[40] D. Adekoya, M. Tahir, N.A.S. Amin, Recent trends in photocatalytic materials for reduction of carbon dioxide to methanol, Renew. Sustain. Energy Rev. 116 (2019), 109389.

[41] M.A. Bezerra, R.E. Santelli, E.P. Oliveira, L.S. Villar, L.A. Escaleira, Response surface methodology (RSM) as a tool for optimization in analytical chemistry, Talanta 76 (5) (2008) 965–977.

[42] T. Xiang, F. Xin, C. Zhao, S. Lou, W. Qu, Y. Wang, Y. Song, S. Zhang, X. Yin, Fabrication of nano copper oxide evenly patched on cubic sodium tantalate for oriented photocatalytic reduction of carbon dioxide, J. Colloid Interface Sci. 518 (2018) 34–40.

[43] S. Zhang, X. Yin, Y. Zheng, Enhanced photocatalytic reduction of CO_2 to methanol by ZnO nanoparticles deposited on ZnSe nanosheet, Chem. Phys. Lett. 693 (2018) 170–175.

[44] E. Bahadori, A. Tripodi, A. Villa, C. Pirola, L. Prati, G. Ramis, N. Dimitratos, D. Wang, I. Rossetti, High pressure CO_2 photoreduction using Au/TiO2: unravelling the effect of co-catalysts and of titania polymorphs, Catal. Sci. Technol. 9 (9) (2019) 2253–2265.

[45] X. Shao, X. Yin, J. Wang, Nanoheterostructures of potassium tantalate and nickel oxide for photocatalytic reduction of carbon dioxide to methanol in isopropanol, J. Colloid Interface Sci. 512 (2018) 466–473.

[46] P. Nagababu, S.A.M. Ahmed, Y.T. Prabhu, A. kularkar, S. Bhowmick, S.S. Rayalu, Synthesis of Ni2P/CdS and Pt/TiO2 nanocomposite for photoreduction of CO_2 into methanol, Sci. Rep. 11 (1) (2021) 8084.

[47] J.O. Olowoyo, M. Kumar, S.L. Jain, J.O. Babalola, A.V. Vorontsov, U. Kumar, Insights into reinforced photocatalytic activity of the CNT–TiO2 nanocomposite for CO_2 reduction and water splitting, J. Phys. Chem. C. 123 (1) (2019) 367–378.

[48] J.O. Olowoyo, M. Kumar, B. Singh, V.O. Oninla, J.O. Babalola, H. Valdés, A. V. Vorontsov, U. Kumar, Self-assembled reduced graphene oxide-TiO2 nanocomposites: synthesis, DFTB+ calculations, and enhanced photocatalytic reduction of CO_2 to methanol, Carbon 147 (2019) 385–397.